

# Application of the Hydrodynamic Theory and the Finite Element Method in the Analysis of Bird Strike in a Flat Barrier

Marinko Ugrčić<sup>1)</sup>

In both cases of the used methods, i.e. theories, the hydrodynamic theory and the finite element method, the bird body was modeled as a porous water-air material in the shape of a flat or hemi-spherically ended cylinder. The finite element bird modeling was carried out by the use of the Smooth Particle Hydrodynamics (SPH) method for materials of different porosity. In this way, the dependence of the sound speed and the bulk modulus on the porosity in the equation of state (EOS) was developed. A new approach to the computation of stagnation pressure in the porous material was proposed as well. On the other hand, the Lagrangian target was considered as a simple flat rigid steel or elastic Al-alloy plate. The comparative analysis of the numerical results of the bird impact for the Hugoniot shock theory and the SPH method was given. Some results of experimental data were also included.

*Key words:* impact, mechanical impact, birds, modelling, process simulation, finite element method, hydrodynamic theory

## Introduction

ONE of possible and very dangerous accidents is a bird strike on the aircraft during the flight. This case is characterized by a high speed impact of the bird onto the aircraft structure causing large dynamic deformations of the elements which may lead to construction disintegration. That is why theoretical research and numerical simulations of the bird strike are very important and should be implemented during the design phase of the aircraft development process [1, 4]. This paper presents some results of the theoretical analysis and the numerical simulations of dynamic loading of the bird body and the flat plate loaded by the bird impact.

Most of the initial models of the bird impact were developed on the basis of the classical impact theory and they used the force-impulse equation. Unfortunately, these models failed to predict the damage to its details. Further, the elementary one-dimensional theory of hydrodynamics was used to study the bird impact. The hydrodynamic theory assumes that during impact at high velocity the bird material tends to behave as a fluid. It means that in a material to flow the stresses generated during impact should exceed the strength of the material, so that the material strength and viscosity are neglected. The mass-momentum-energy conservation equations and a simple pressure-density-energy equation of state were used to describe the material behaviour [5, 6]. A more appropriate interpretation of the bird strike was carried out by involving the shock wave theory.

Regarding the finite element method, three approaches have been successfully employed to simulate this phenomenon. These are the Lagrangian, Arbitrary Lagrangian-Eulerian (ALE) and SPH formulations.

The Lagrangian formulation is based on Lagrangian mechanics, and was the earliest approach to be used in the bird strike analysis [7, 8]. In Lagrangian analyses, the bird is divided into elements and the element mesh is bounded to the

material. Birds undergo extreme deformation during strikes, and this can cause problems in the Lagrangian meshes as some elements may experience negative volumes. Solving dynamic transient nonlinear problems requires a time step that is often a function of the aspect ratio of the smallest element in the mesh. This causes further problems during high distortion in the Lagrangian analysis because the time step may become unacceptably small.

The ALE method allows space to contain more than one material (e.g. water and air) and uses arbitrary reference coordinates that allow the material to flow through the Euler mesh rather than the proper moving of the Lagrange material mesh [7, 9]. It does not experience a time step problem, but high distortion can still cause negative volume issues.

The SPH formulation is a more recently developed finite element method that uses particles of mass rather than an element mesh to represent the bird [10-12]. Regarding the Lagrangian method, the SPH avoids problems caused by mesh distortion. The comparison of the ALE and SPH methods (Fig.1) shows a more appropriate physical appearance of the process given by the SPH interpretation.

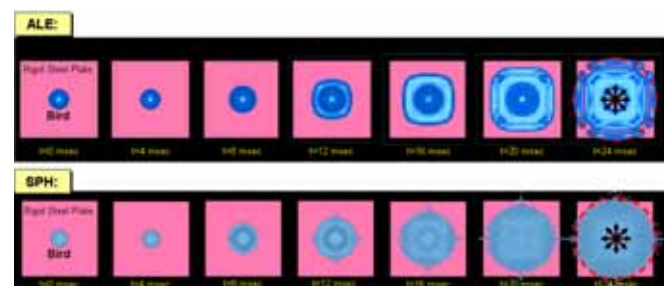


Figure 1. Comparison of ALE and SPH bird impacts on a rigid plate

Finally, let us say that the International Birdstrike Research Group (IBRG) developed a set of standardized artificial bird designs to be used in real tests, all regarding

<sup>1)</sup> Mathematical Institute SASA, Kneza Mihaila 36, 11000 Belgrade, SERBIA

possible situations of strikes of extremely large birds. The tests were based on the biometric parameters of the thirty struck bird species, and it was concluded that flat ended cylinders, hemi-spherically ended cylinders and ellipsoid shapes may be suitable to represent the bird body depending on the bird species [12].

The basic goals of the research presented in this work can be summarized as follows:

- brief retrospective of the bird strike hydrodynamic theory coupled with shock wave equations and the definition of the elastic bulk modulus and the sound speed of porous medium depending on its proper porosity,
- numerical simulation of various cases of bird impacts including the variation of bird material density, shape and impact velocity, impact angle and parameters of the target plate, and
- comparison of some results of the numerical simulation and the experimental testing.

### Elementary shock theory of the bird strike

#### Description of impact

Figure 2 depicts four phases of the impact of a cylindrical body of fluid onto a rigid target at an oblique angle of  $90^\circ$ . More complex geometries, such as hemi-spherically ended cylinders, complicate the theory but behave in the same broad manner.

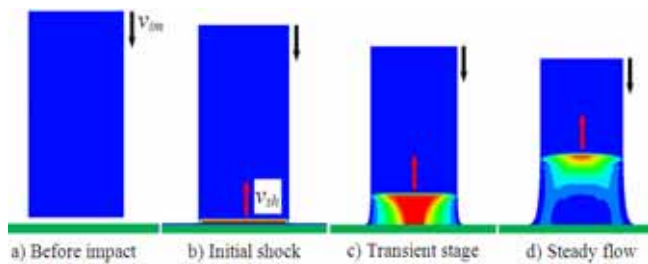


**Figure 2.** Impact phases of a fluid cylinder given by the numerical simulation

The four phases (Fig.2) can be described as follows:

- a) The cylinder of fluid approaches the flat target at an oblique angle and with a purely axial velocity. Its internal pressure is equal to that of the ambient atmosphere.
- b) The leading face of the cylinder strikes the target and its constituent particles are instantaneously stopped, creating a violent shock wave – the Hugoniot shock – that travels back along the length of the cylinder as adjacent particles are brought to rest. The shocked region behind the wave is subject to a transient Hugoniot pressure of high magnitude.
- c) The huge pressure gradient between the radially unconfined free surface of the shocked region and its interior causes the generation of release waves which trigger rapid radial expansion at the shocked end. The release or decompression waves travel at the speed of sound back towards the centre of the cylinder, reducing the strength of the Hugoniot shock wave as they progress.
- d) The transient period ends when the release waves meet at the cylinder's central axis [13]. A steady flow is established as the cylinder flows onto the surface of the target. A steady stagnation pressure is reached, with its maximum at the centre of impact. The impact forces decay completely once the fluid's

velocity is entirely radial.

#### EOS of water and air

Additional useful information resulting from associating the bird to the water is the equation of state (EOS) used to describe the pressure-density ( $p$ - $\rho$ ) relationship in the bird medium. A few equations are available and the one most commonly used for the water-bird is a polynomial of degree 3 [4, 7]. This polynomial EOS for the bird model corresponds to a hydrodynamic, isotropic, and non-viscous constitutive law and is given as follows:

$$p = C_0 + C_1\mu + C_2\mu^2 + C_3\mu^3 + (C_4 + C_5\mu + C_6\mu^2)E \quad (1)$$

$$\mu = \frac{\rho}{\rho_0} - 1 \quad (2)$$

where is:  $C_0$ - $C_6$  - coefficients of the polynomial equation,  $E$  - internal energy and  $\mu$  - the change in density during the impact.

The coefficients are given by expressions based on the initial density, the speed of sound in the medium and an experimental constant  $k$ . With a known and negligible initial equilibrium pressure, the values of the coefficients in Eq.1 are given as follows:

$$C_1 = \rho_0 c_0^2 \quad (3)$$

$$C_2 = (2k-1)C_1 \quad (4)$$

$$C_3 = (k-1)(3k-1)C_1 \quad (5)$$

$$C_0 = C_4 = C_5 = C_6 = 0 \quad (6)$$

where is:  $\rho_0$  - density of the medium (for the water  $\rho_{0,w} = 1000 \text{ kg/m}^3$  and for the air  $\rho_{0,a} = 1.225 \text{ kg/m}^3$ ),  $c_0$  - speed of the sound in the medium (for the water  $c_{0,w} = 1483 \text{ m/s}$  and for the air  $c_{0,a} = 342 \text{ m/s}$ ) and  $k$  - experimental constant (for the water  $k_w = 2.0$  and for the air  $k_a = 1.03$ ).

The air is modeled by using the Gamma Law of EOS, given from Eq.1, as follows:

$$C_4 = C_5 = 0.4 \quad (7)$$

$$C_0 = C_1 = C_2 = C_3 = C_6 = 0 \quad (8)$$

#### EOS of porous material

The EOS of porous material is based on the thermodynamic equation that describes the state of matter under a given set of physical conditions. It is a constitutive equation that provides a mathematical relationship between two or more state functions such as the temperature  $T$ , the volume  $V$  or density, pressure and internal energy:

$$p = p(\rho, E) = p(V, E) = p(\rho, T) = p(V, T) \quad (9)$$

Further development of the theory for porous medium requires the elastic bulk modulus and the sound speed of porous to be defined. The sound speed is calculated assuming:

$$c_{por} = (1-z)^m c_{0,w} + z c_{0,a} \quad (10)$$

The diagram in Fig.3 illustrates the developed distribution for the exponent values  $m=1-5$ , and  $m=10$ .

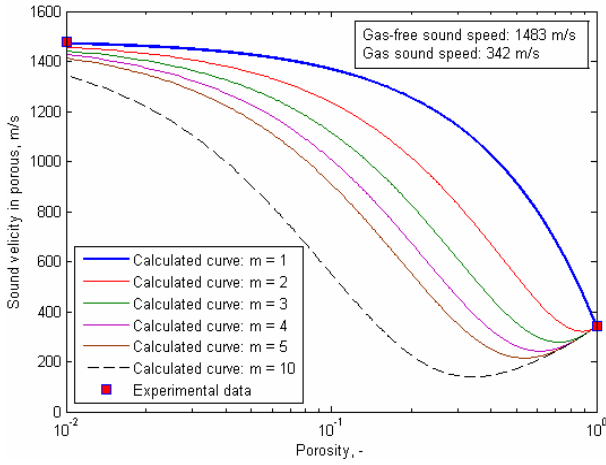


Figure 3. Sound speed distribution depending on porosity

Using a well-known sound speed - elasticity relation for the fluid medium, the distribution of the bulk modulus depending on porosity was calculated and shown in Fig.4. In such a way, the determined relevant mechanical parameters are used in the solver P-alpha EOS for the porous material.

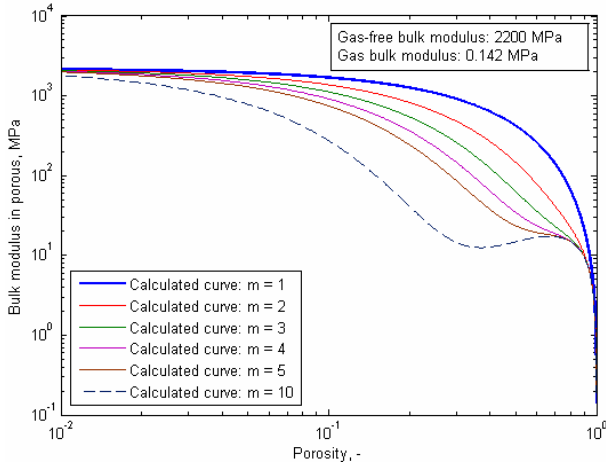


Figure 4. Bulk modulus distribution depending on porosity

However, one precise EOS for the real state definition of the impact is not possible without the shock phase analysis based on the hydrodynamic shock wave theory. The EOS model formulation for the shock or the Hugoniot phase is presented below.

#### Shock pressure and shock velocity

A bird undergoing impact at high velocity behaves as a highly deformable projectile where the yield stress is much lower than the sustained stress. Accordingly, the impact can be qualified as a hydrodynamic impact. This, and the fact that the density of flesh is generally close to the density of water, makes it possible for a bird to be considered as a lump of water hitting a target. This is the main assumption leading to the understanding of the behaviour of the bird.

In the case of low impact velocities, i.e. at the loads below the Hugoniot limit, the single elastic wave propagates through the bird material. The speed of the elastic wave followed by the small perturbations of the bird body particles is equal to the sound velocity in the fluid:

$$c_E = \sqrt{\frac{K}{\rho_0}} \quad (11)$$

where is:  $c_E$  - the sound speed in the fluid and  $K$  - the elastic bulk modulus of the fluid (for the water  $K = 2.2$  GPa).

At higher impact velocities, the Hugoniot shock wave appears. The initial shock and the steady flow phases of the bird strike event will be thus considered in detail. The pressure of the initial shock, the so-called Hugoniot pressure, for incompressible and compressible bird material, is given by the following equations, respectively:

$$p'_{sh} = \rho c_0 v_{im} \quad (12)$$

$$p_{sh} = \rho v_{sh} v_{im} \quad (13)$$

where is:  $p_{sh}$  - the shock pressure,  $c_0 = c_E$  - the sound speed in the fluid,  $v_{sh}$  - the shock velocity of the generated shock wave,  $v_{im}$  - the translational particle velocity or, simply, the projectile velocity and  $\rho_0$  - the initial density.

The variations of the shock pressure in the water depending on the impact velocity, according to Eqs. (12) and (13), are shown in Fig.5.

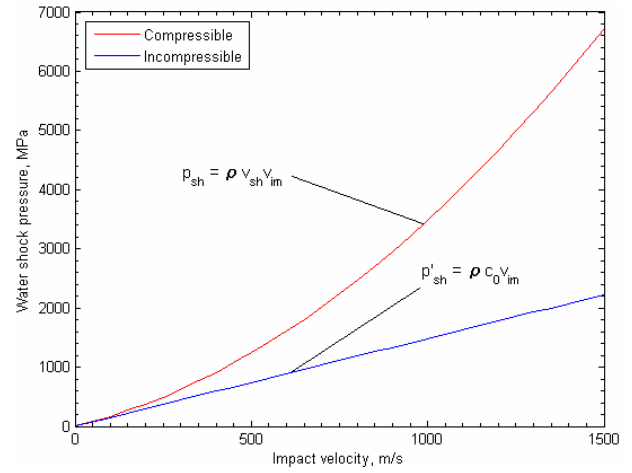


Figure 5. Shock pressure in the water depending on the impact velocity

The pressure of the steady flow  $p_{stag}$  (stagnation pressure) is calculated according to Bernoulli and is given by the equation:

$$p_{stag} = \frac{1}{2} \rho v_{im}^2 \quad (14)$$

Analytically, these two pressures are important since the Hugoniot pressure gives the maximum possible value for the impact at its very beginning and the stagnation pressure gives the expected reading when the flow stabilizes. It is also important to realize that the pressure is independent of the size of the projectile since the mass is not a variable in the pressure equations. This implies that the pressure results are the same regardless of the projectiles, provided they share the same impact velocity. Of course, the force and energy of a bigger projectile are proportionally larger and will cause more damage.

The values of the variables needed to calculate the stagnation pressure are easily available. On the other hand, the Hugoniot pressure depends on the impact velocity and the shock velocity which itself also depends on the impact velocity. Moreover, the equation changes whether or not porosity is included, or if the fluid considered is water or a substitute.

The equations given below apply to the bird-body with an amount of the air mixed in, also called porosity, since experience has shown that porosity has a non-negligible

effect on overall results and is closer to the behaviour of a bird upon impact [5, 7]:

$$\rho_1 v_{sh} = \rho_2 (v_{sh} - v_{im}) \quad (15)$$

$$p_1 + \rho_1 v_{sh}^2 = p_2 + \rho_2 (v_{sh} - v_{im})^2 \quad (16)$$

$$\frac{\rho_1}{\rho_2} = (1-z) \left( \frac{p_2}{A} + 1 \right)^{\frac{-1}{4k-1}} + z(1-q) \quad (17)$$

$$A = \frac{\rho_1 c_0^2}{4k-1} \quad (18)$$

$$\frac{\rho_2}{\rho_1} = \frac{1}{1-q} \quad (19)$$

where is:  $\rho_1$  and  $\rho_2$  - the density of the medium before and after the impact,  $p_1$  and  $p_2$  - the pressure before and after the impact ( $p_1$  is negligible) and  $z$  - the contribution of the air mixed in the medium (amount of the material porosity).

The parameter  $q$  is defined as:

$$q = 1 - \frac{\rho_1}{\rho_2} = q_1 - q_2 \quad (20)$$

where is:

$$q_1 = \left( \frac{2\bar{p}k_a + \frac{\rho_1 c_{0,a}^2}{p_1}}{2\bar{p}k_a^2} \right) \quad (21)$$

$$q_2 = \left[ \frac{\left( 2\bar{p}k_a + \frac{\rho_1 c_{0,a}^2}{p_1} \right)^2 - 4\bar{p}^2 k_a^2}{2\bar{p}k_a^2} \right]^{\frac{1}{2}} \quad (22)$$

$$\bar{p} = \frac{p_2}{p_1} = \frac{\rho_1 c_{0,a}^2}{p_1} \frac{q}{(1-k_a q)^2} \quad (23)$$

For the air, the typical pressure-density relation for a shock compression used by many researchers is given by:

$$\frac{\rho_2}{\rho_1} = \frac{1 + \left( \frac{\gamma+1}{\gamma-1} \right) \frac{p_2}{p_1}}{\left( \frac{\gamma+1}{\gamma-1} \right) + \frac{p_2}{p_1}} \quad (24)$$

where is:  $\gamma$  - the ratio of specific heat ( $\gamma = 1.4$  for the air).

Applying the mixture theory [3] and combining Eqs. (23) and (24), the EOS for the shock compression phase of the porous material was derived. This EOS is given by:

$$\left( \frac{\rho_1}{\rho_2} \right)_{porous} = (1-z) \left( \frac{\rho_1}{\rho_2} \right)_{water} + z \left( \frac{\rho_1}{\rho_2} \right)_{air} \quad (25)$$

Finally, using Eq. (16), the above equation becomes:

$$\frac{\rho_{1,porous}}{\rho_{2,porous}} = (1-z) \left( \frac{p_2}{A} + 1 \right)^{\frac{-1}{4k-1}} + z(1-q) \quad (26)$$

The solution for the shock velocity in the porous is found by isolating  $p_2$  and  $\rho_2$  after the shock and by the simultaneous solution of equations (15), (16) and (26).

Once the shock velocity is known, the Hugoniot pressure can be found from (13). Figures 6 and 7 show the shock velocity and the shock pressure for the impact velocities ranging from 0 to 500 m/s. The shock velocity and the shock pressure are plotted for four different porosities ( $z=0.1$  to 0.4) in order to illustrate the influence of that parameter.

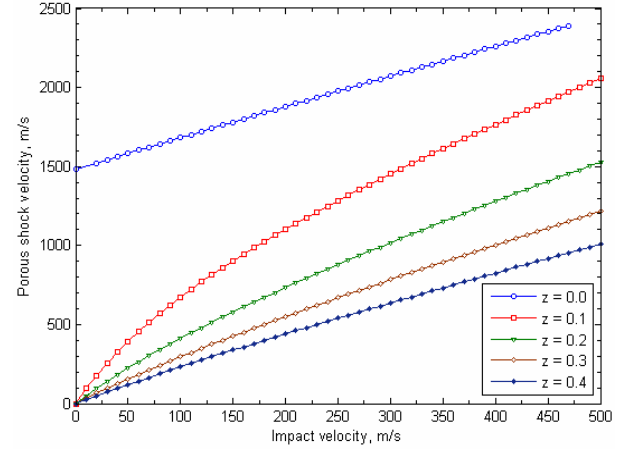


Figure 6. Theoretical dependence of shock velocity on porosity

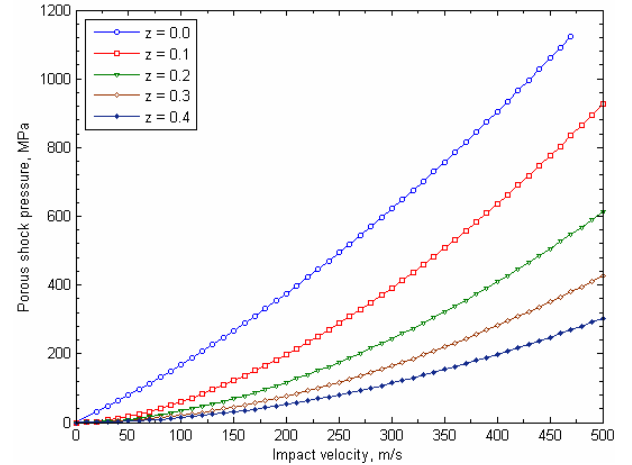


Figure 7. Theoretical dependence of shock pressure on porosity

### Stagnation pressure in the steady flow regime

For an incompressible fluid like water, Eq.14 is valuable. However, in compressible materials density increases with pressure and produces higher values of the stagnation pressure. In the case of compressible porous material, we assume that the increasing factor equals  $(1-z)^{-1}$ :

$$p_{stag,z} = \frac{1}{1-z} \rho_{porous} \frac{v_{im}^2}{2} \quad (27)$$

$$\rho_{porous} = (1-z) \rho_{water} + z \rho_{air} \quad (28)$$

The diagram in Fig.8 illustrates the stagnation pressure distribution depending on porosity and impact velocity.

When the fluid flow reaches a steady state, it is also possible to calculate the pressure distribution along the radius, assuming the exponential functional dependence:

$$p = p_{stag} e^{\left[-\frac{1}{2} \left(\frac{r}{R}\right)^2\right]} \quad (29)$$

where is:  $r$  - the radial position and  $R$  - the radius of the bird body.

This dependence is shown in Fig.9 for the stagnation pressure calculated on the basis of Eq. 14.

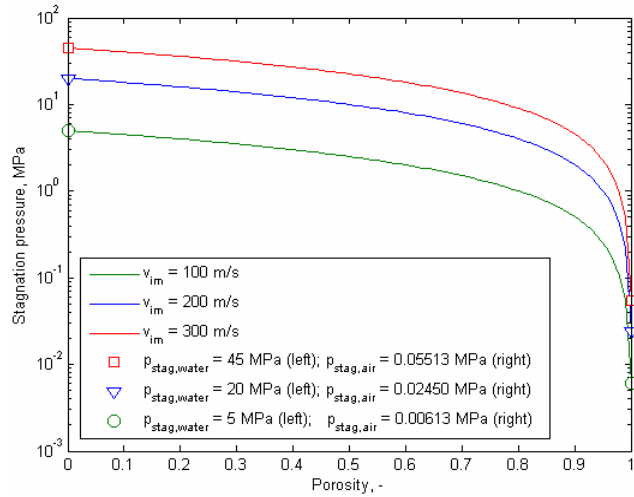


Figure 8. Stagnation pressure vs. impact velocity and porosity

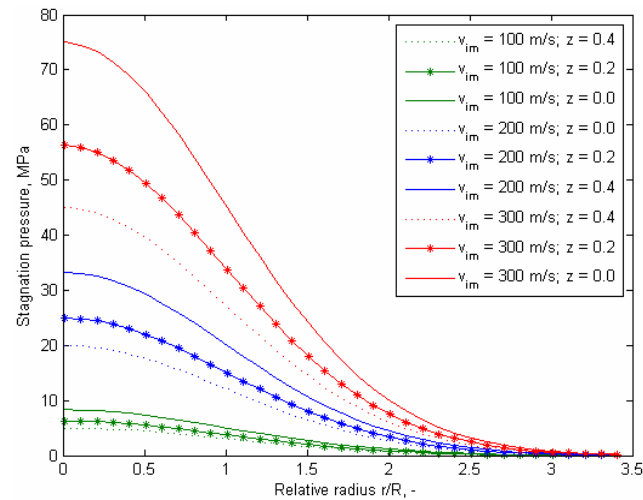


Figure 9. Stagnation pressure distribution along the radius vs. impact velocity and porosity

Involving Eq.27 in Eq.29, we would get a normalized diagram of the stagnation pressure distribution with a reduced number of curves in Fig.9. In this case, the stagnation pressure for the same impact velocity would be identical and represented by a solid line. It means that the stagnation pressure does not depend on porosity and that the pressure distribution is the same regardless of porosity.

## FEM modeling

### Bird model

For a *bird material* a homogeneous mixture of water and air was used. The porosity (volume presence of the air) varied from  $z = 0.0$  to  $z = 0.4$ . The effect of porosity with the P-alpha EOS for porous material was investigated. The appropriate mechanical parameters of the water and the water-air mixture depending on porosity are given in Table 1.

Table 1. Mechanical parameters of the water and the water-air mixture

Porosity $z$	Density $\rho$	Sound speed $c_p$ (for $m=1$ )	Bulk modulus $K$ (for $m=1$ )
-	kg/m <sup>3</sup>	m/s	MPa
0.0	1000.0	1483	2200
0.1	900.12	1368	1668
0.2	800.25	1256	1260
0.3	700.37	1142	907
0.4	600.49	1026	632

For the purpose of this research, two typical *bird shapes* generally used in the bird strike analysis, a flat and a hemispherical cylinder, were considered. In each case, the height and the diameter of the bird was assumed to be 200 mm and 100 mm, respectively. The length-to-diameter ratio of 2 for each bird shape was identical.

Two types of the numerical models of body shapes based on the SPH particles distributions along the symmetry axis are presented in Fig.9.

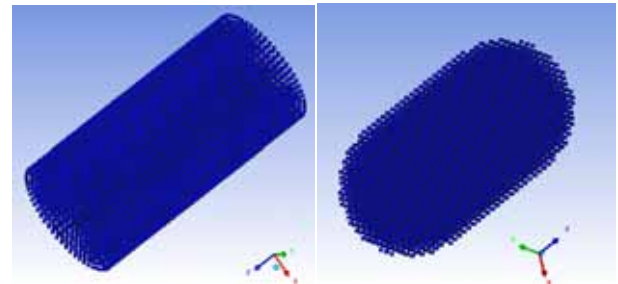


Figure 9. The SPH particles distribution along the symmetry axis of the hemi-spherically ended cylinder: axial (left) and radial (right)

The cylindrical projectile model had a total of 12640 SPH particles and the cylinder with the hemi-spherical ends model had a total of 10512 SPH particles. The numerical models of the bird body were built such that the nodal density of each body was approximately the same [3, 6].

### Target model

For simplicity, the target structure was initially assumed to be rigid for the comparative analysis of the shock pressures and the shock wave velocities. In addition, the impact velocity was assumed to be normal to the target.

To simulate a rigid target, the target structure was modeled as a steel plate, with the dimensions 800 × 800 mm and a thickness of 10 mm. All degrees of freedom of the target structure were constrained. The target structure was modeled using the Belytschko-Tsay shell elements (Fig.10).

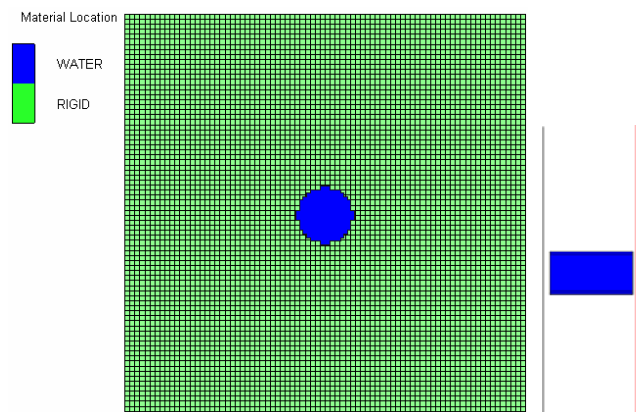


Figure 10. Lagrangian model of a rigid target and an SPH model of a cylindrical bird projectile

The target flexibility was introduced into the analysis, and the inherent coupling between the impact loads and the target deflection was explored. The appropriate mechanical parameters of the Al alloy are given in Table 2.

**Table 2.** Mechanical parameters of the Al alloy target structure

Density $\rho$	Poisson's ratio $\mu$	Young's modulus $E$	Shear modulus $G$	Tensile yield strength $R_{eH}$
kg/m <sup>3</sup>	-	GPa	GPa	MPa
2.785	0.33	71.00	28.60	280.00

Besides the frontal impact, the effects of the oblique impact onto the flexible target were considered. Specifically, a bird projectile direction of 45 degrees was simulated.

### Results and discussion

#### Effect of the projectile shape on a rigid target

Body deformations of the artificial bird at different stages of the impact process are presented for various projectile shapes investigated in Figures 11 and 12.

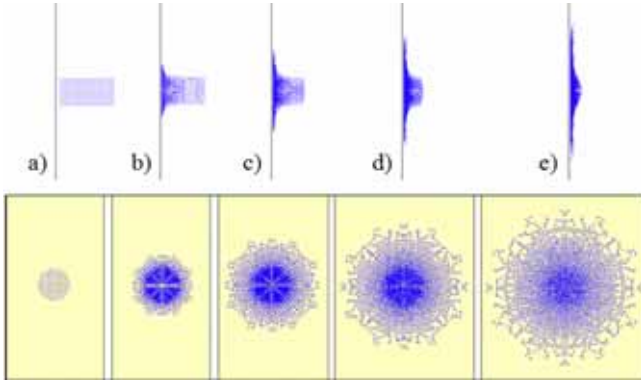


**Figure 11.** Deformations of the cylindrical SPH body at different times during the impact with a rigid flat target ( $t = 0.0, 0.5, 1.0, 1.5, 2.0$  ms)

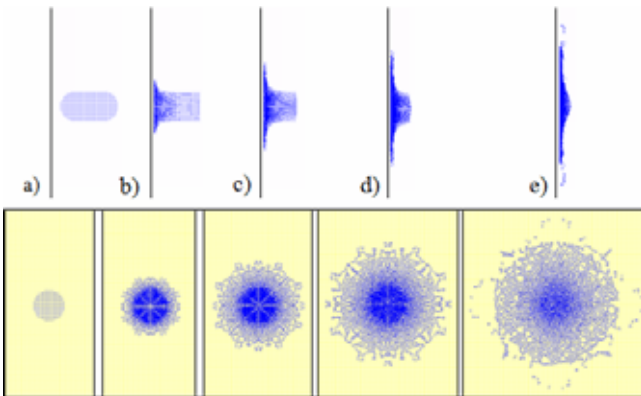


**Figure 12.** Deformations of the hemispherical cylinder SPH body at different times during the impact with a rigid flat target ( $t = 0.0, 0.5, 1.0, 1.5, 2.0$  ms)

#### Shock pressure and shock velocity

The impact velocity for all bird projectiles varied from 100 m/s to 500 m/s and was normal to the rigid target. In addition, all the projectiles were assumed to have a porosity  $z$  of 0.

A typical history diagram of the shock pressure distribution in the frontal plane of the cylindrical body for velocities of 200 and 300 m/s impact are shown in Fig. 13.

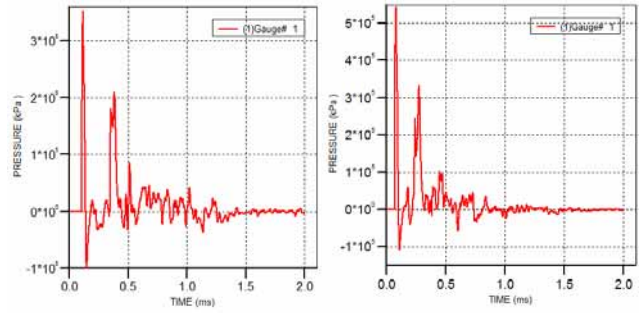


**Figure 13.** Shock pressure distribution along the radius for different impact velocities:  $v_{im} = 200$  m/s (left) and  $v_{im} = 300$  m/s (right)

The history diagrams in Fig.13 are similar and show appearances of two peaks on each shock pressure curve that is typical for two-phase materials such as a porous one.

The SPH computed shock pressures for the cylindrical bird shape are presented in Fig.14 and 15, for an appropriate range of projectile velocities and porosity. This last one also displays the experimental results from [5] for medium size birds. The exact weights of the test specimens were not given; however, it is stated that the specimens weighed between 0.5 kg to 1 kg. In addition, these figures display the computed shock pressures based on Wilbeck's theory [3].

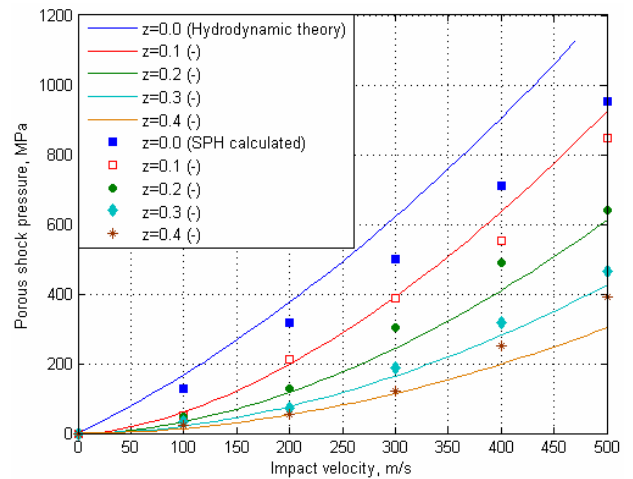


**Figure 14.** Comparison of the hydrodynamic theory and the SPH calculated data for the shock pressure distribution vs. impact velocity and porosity

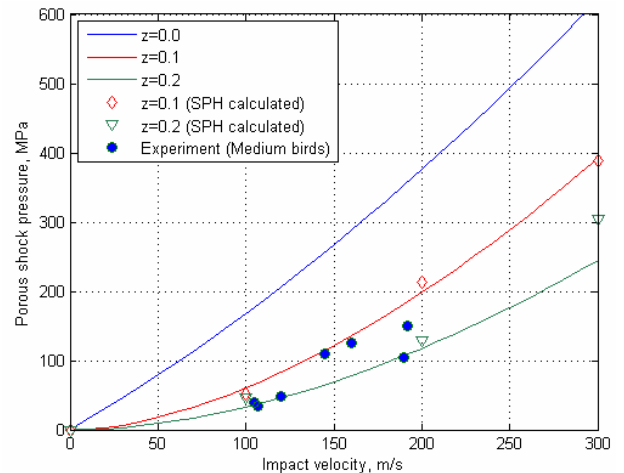


**Figure 15.** Computed and experimental data for the shock pressure distribution vs. impact velocity and porosity

The analysis of shock pressures calculated on the basis of the hydrodynamic theory and the SPH method (Fig.14) shows a good correlation of the computed data, especially for lower values of impact velocities ( $v_{im} < 300$  m/s). Further increasing of impact velocity causes a higher deviation of the computed shock pressures.

Furthermore, the distribution of the computed and experimental data in Fig.15 for the shock pressure in the porous medium, confirms the validity of the predictive principle assuming the bird body as a porous medium.

#### Stagnation pressure in the steady flow regime

The steady-state flow pressure stage is considered to be more critical for bird impact events. A simplified shock pressure distribution is used to determine the stagnation pressure in the steady flow regime. This diagram, implemented in the pressure history record given by the numerical simulation for 100 m/s impact velocity, will have the form shown in Fig.16 (a smooth thick line).

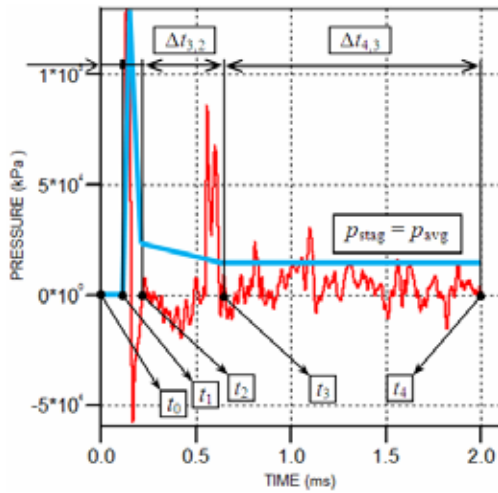


Figure 16. Simplified shock pressure distribution with typical stages

The typical stages of the pressure-time response are:  $\Delta t_{1,0}$  - stage before impact,  $\Delta t_{2,1}$  - shock wave stage;  $\Delta t_{3,2}$  pressure release stage and  $\Delta t_{4,3}$  - steady-state flow regime.

Stagnation pressure is calculated, based on the equations:

$$p_{stag} = \frac{I_{sp}}{\Delta t_{4,3}} \quad (30)$$

$$I_{sp} = \int_{t_3}^{t_4} p dt \quad (31)$$

$$\Delta t_{4,3} = \Delta t_{4,1} - \Delta t_{3,1} = \frac{L}{v_{im}} - \Delta t_{3,1} \quad (32)$$

where is:  $I_{sp}$  - the specific impulse of the shock pressure during the stagnation stage,  $\Delta t_{4,1}$  - the impact duration or a so-called bird "squash-up" time,  $L$  - the length of the bird body and  $\Delta t_{3,1}$  - the time sequence of the shock wave stage (up to 30% of the impact time).

Finally, the integral of the pressure during the steady state stage (Eq.31), calculated automatically by the integration of the pressure response diagram (e.g. in Fig.16), is given in Fig.17.

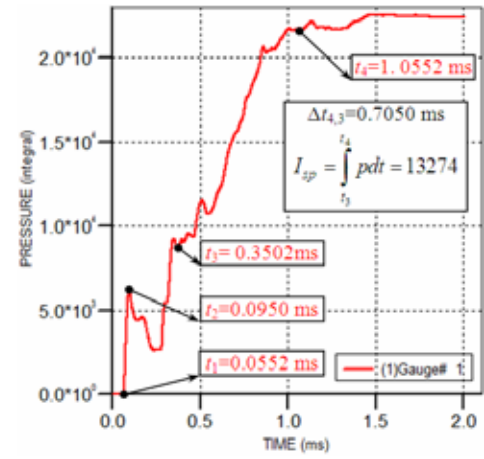


Figure 17. Shock pressure integral vs. time at 200 m/s impact velocity

The stagnation pressure computed for the case of a cylindrical bird shape is presented in Fig.18, for a range of projectile velocities at  $z = 0.4$ . This figure displays the experimental results from [7, 13] for medium size birds as well.

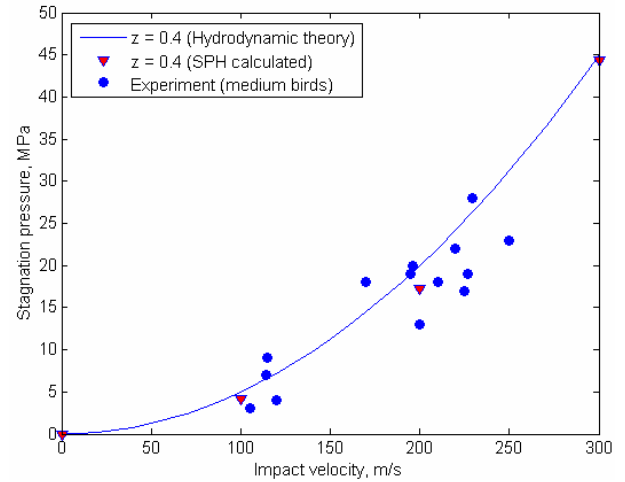
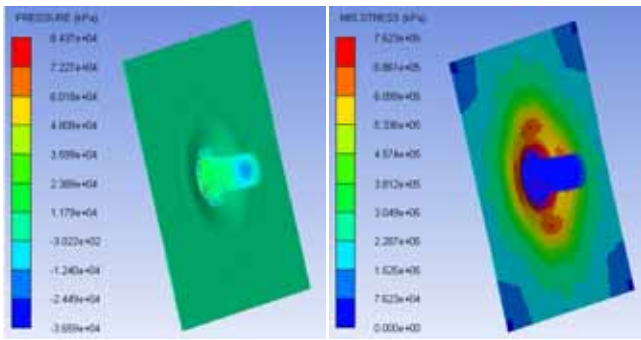


Figure 18. Stagnation pressure distribution vs. impact velocity for  $z = 0.4$

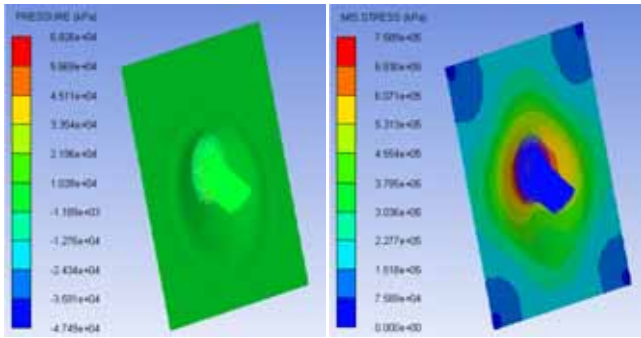
Fig.18 shows that the computed steady state pressure from the cylindrical projectile shape matches well with the experimental results. Most previous analyses [2, 5, 7, 13] were capable of predicting the steady state stagnation pressure with good accuracy. In fact, Wilbeck's one-dimensional theory provides a quick way of checking the steady state pressure before performing a full numerical three-dimensional analysis.

#### Effect of the target flexibility on the impact loads and deformations

The shell model of an Al alloy plate, 3 mm of thickness and with the mechanical parameters given in Table 2, was used to show the effect of the target flexibility on the impact loads and plate deformations. The boundary conditions assumed that all edges of the plate were fixed against displacement in any directions. Besides the frontal impact, the effects of the oblique impact ( $\alpha = 45^\circ$ ) on the flexible target were considered. The pressure and the von Mises stress distributions for the Al plate at an impact velocity of 300 m/s are shown in Fig.19.



a) Orthogonal bird impact ( $\alpha = 90^\circ; z = 0.2; t = 0.3 \text{ ms}$ )



b) Oblique bird impact ( $\alpha = 45^\circ; z = 0.2; t = 0.5 \text{ ms}$ )

**Figure 19.** Pressure and von Mises stress distributions in the metallic plate at a cylinder impact velocity of 300 m/s.

Regarding the pressure distribution in both orthogonal and oblique impact (Fig.19) at the moment when the full contact surface will be reached, the appearance of lower pressures characterizes the oblique impact caused by the enlarged contact surface at  $\alpha = 45^\circ$ . However, the comparative analysis of the von Mises stress distributions in the metallic plate shows no difference between the stress values for the orthogonal impact and the oblique one.

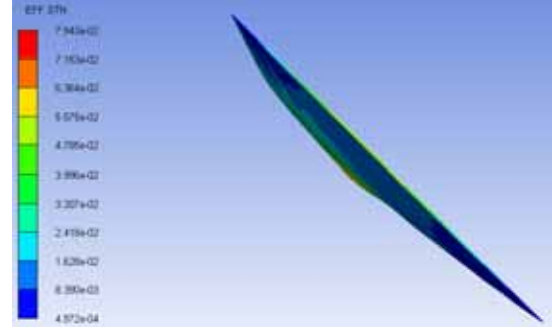
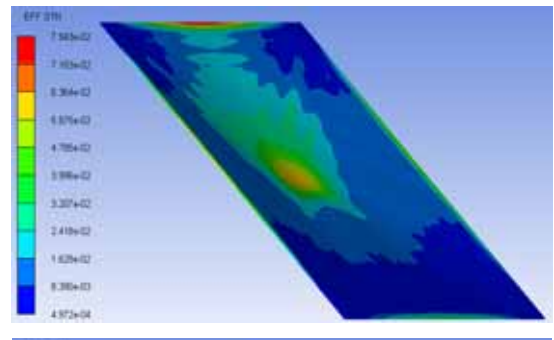
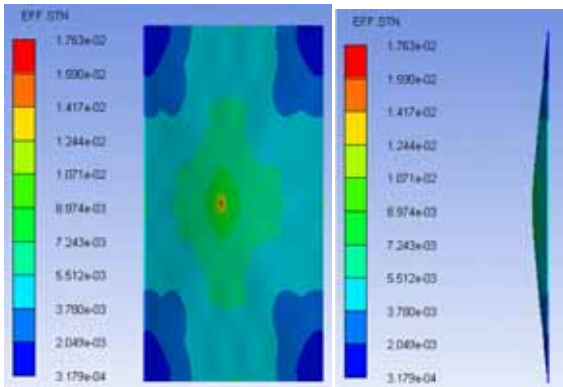


**Figure 21.** Effective strain distribution along a 3 mm thick Al alloy plate for the oblique cylinder impact ( $v_{im} = 300 \text{ m/s}; z = 0.2; T = 1.5 \text{ ms}$ ).

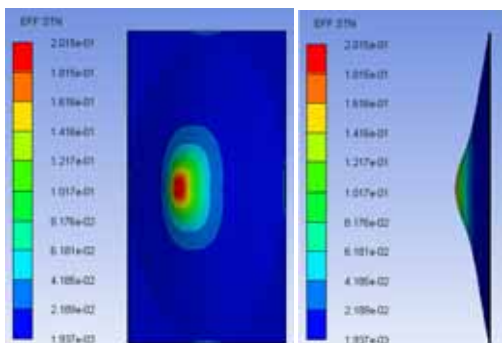
The effective strain distributions along the 3 mm thick Al alloy plate for the orthogonal and oblique impact depending on the impact velocity are shown in Figures 20 and 21, respectively.

Figures 20 and 21 show that the predicted effective strain for the cylindrical bird body decreases with the obliquity of impact velocity.

Finally, the pressure, the von Mises stress and the effective strain distributions are tested at the same impact conditions as for the hemispherical cylinder bird body. The results of the numerical simulations are given in Figures 22, - 24, respectively.

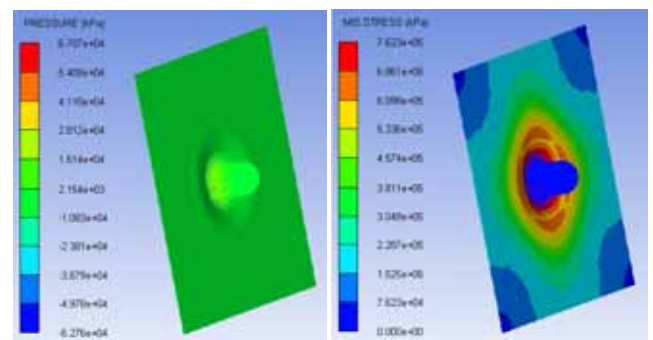


a)  $v_{im} = 100 \text{ m/s}, z = 0.2; t = T = 2 \text{ ms}; 60^\circ \text{ view direction (left); side view (right)}$

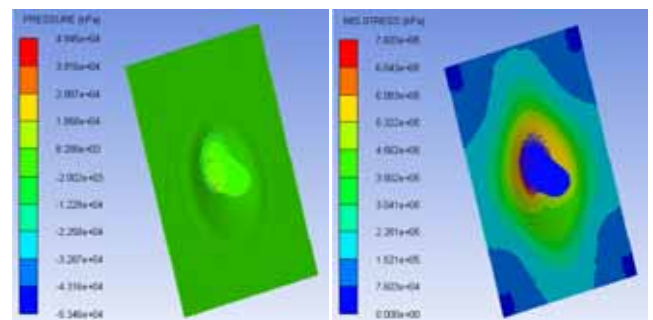


b)  $v_{im} = 300 \text{ m/s}; z = 0.2; t = T = 1 \text{ ms}; 60^\circ \text{ view direction (left); side view (right)}$

**Figure 20.** Effective strain distribution along a 3 mm thick Al alloy plate for the orthogonal cylinder impact depending on the impact velocity.

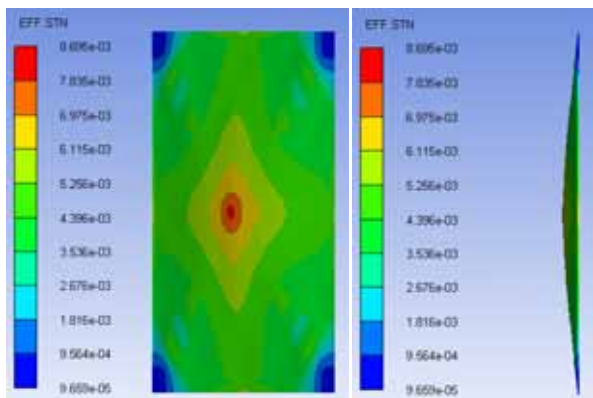


a) Orthogonal bird impact ( $\alpha = 90^\circ; z = 0.2; t = 0.3 \text{ ms}$ )

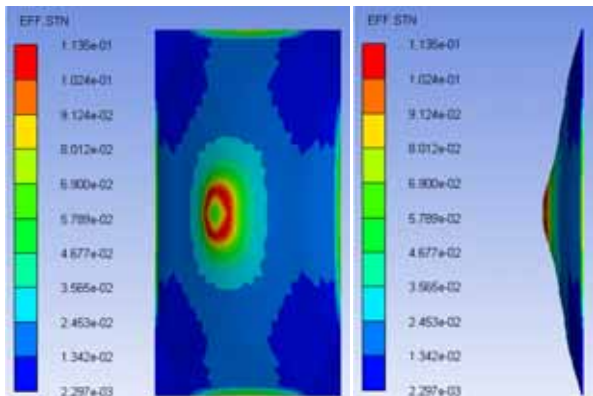


b) Oblique bird impact ( $\alpha = 45^\circ; z = 0.2; t = 0.5 \text{ ms}$ )

**Figure 22.** Pressure and von Mises stress distributions in the metallic plate at a hemispherical cylinder impact velocity of 300 m/s.



a)  $v_{im} = 100$  m/s,  $z = 0.2$ ;  $t = T = 2$  ms;  $60^\circ$  view direction (left); side view (right)



b)  $v_{im} = 300$  m/s;  $z = 0.2$ ;  $t = T = 1$  ms;  $60^\circ$  view direction (left); side view (right)

**Figure 23.** Effective strain distribution in a 3 mm thick Al alloy plate for the orthogonal hemispherical cylinder impact depending on impact velocity.

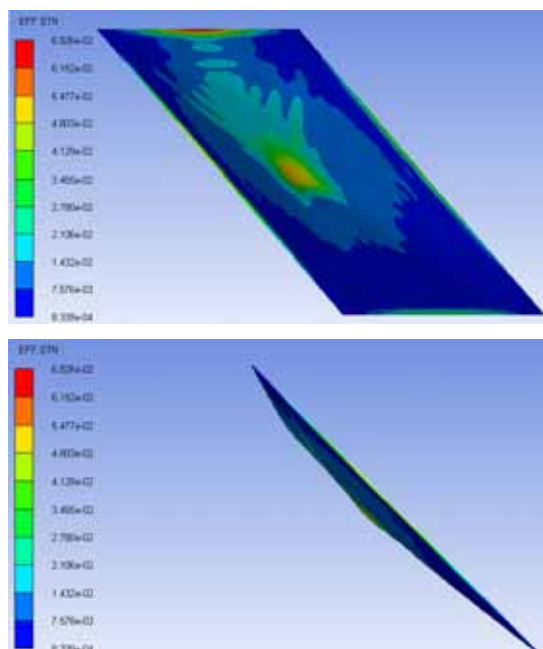


**Figure 24.** Effective strain distribution along a 3 mm thick Al alloy plate for the oblique hemispherical cylinder impact ( $v_{im} = 300$  m/s;  $z = 0.2$ ;  $T = 1.5$  ms).

Comparing the results of the numerical simulations of the bird impact on the deformable target, for a flat cylinder and a hemispherical cylinder shape of the bird body, gives the following:

- Maximum pressure distributions of the flat cylinder

impact (Fig.19 and 22) show 26% higher pressure values than in the case of the orthogonal hemispherical cylinder impact and 38% higher pressure values than in the case of the oblique hemispherical cylinder impact;

- Von Mises stress distributions in the metallic plate (Fig.19 and 22) are practically identical in relation to the stress values for the orthogonal and oblique impact; and
- Effective strain distributions (Fig.20-24) show generally that the reduction of the impact angle results in strain decreasing; regarding the body shape, this means 44% lower values of the maximum strain in the case of the orthogonal hemispherical cylinder impact and 14% lower values of the maximum strain in the case of the oblique hemispherical cylinder impact, all at  $v_{im}=300$ m/s.

## Conclusion

A brief retrospective of the bird strike hydrodynamic theory coupled with the Hugoniot shock wave equations was given. A homogeneous water-air mixture was used for the bird material and the equation for the elastic bulk modulus and the sound speed of porous medium depending on porosity was involved in the analysis.

Finite element numerical simulations of the bird impact were carried out by the SPH method to represent the bird body. Based on the mechanical parameters, determined by the proposed equation, the effect of porosity with the P-alpha EOS for porous materials was tested.

The numerical simulation of various cases of the bird impact including the variation of bird material density, shape and impact velocity, impact angle and target plate parameters was successfully performed.

After comparing some results of the numerical simulation and the experimental testing, it appears that increasing the porosity might produce a better match of the predicted Hugoniot shock and the FEM pressures with those observed in the experiments. In addition, the computed stagnation pressures in the steady state regime, calculated by the proposed method, match well with the experimental results.

Regarding the shape, it can be seen that the predicted shock pressures associated with all bird shapes produced a good correlation with the experimental results.

In the end, the pressure, the von Mises stress and the effective strain distributions in the deformable plate depending on the impact velocity and the impact angle were successfully tested by the SPH method.

## Acknowledgement

Parts of this research were supported by the Ministry of Education and Science of the Republic of Serbia through the Mathematical Institute SANU Belgrade, Grant OI174001 (2011.– 2014.) "Dynamics of hybrid systems with complex structures, Mechanics of materials". The author would like to thank Dr Milan Bojanović, Director of CAD PROFESSIONAL SYS, for his support of the research and for facilitating the use of the licensed academic software ANSYS products.

## References

- [1] MEO, M., VIGNJEVIĆ, R., MAENGO, M.: *Numerical simulations of low-velocity impact on an aircraft sandwich panel*, Composite Structures, 2003, 62, pp.353–360.
- [2] VIGNJEVIĆ, R., ĐORĐEVIĆ, N.: *Modelling of High Velocity Impact on Carbon Fibre Composite Materials*, Scientific Technical

- Review, ISSN 1820-0206, 2010, Vol. 60, No.3-4, pp.3-8.
- [3] UGRČIĆ, M., UGRČIĆ, D.: *FEM Techniques in Shaped Charge Simulation*, Scientific Technical Review, ISSN 1820-0206, 2009, Vol. LVIX, No.1, pp.26-34
- [4] IVANČEVIĆ, D., SMOJVER, I.: *Hybrid approach in bird strike damage prediction on aeronautical composite structures*, Composite Structures, 2011, 94, 1, pp.15-23.
- [5] WILBECK, J.S., RAND, J.L.: *The Development of substitute bird model*, ASME Journal of Engineering for Power, 1981, Vol.103, pp.725-730.
- [6] LAVOIE, M.A., GAKWAYA, A., ENSAN, M.N., ZIMCIK, D.G.: *Review of existing numerical methods and validation procedure available for bird strike modeling*, International Conference on Computational & Experimental Engineering and Sciences, 2007, pp.111-118.
- [7] NIZAMPATMAN, L.S.: *Models and methods for bird strike load predictions*, PhD Dissertation, Faculty of Graduate School, Wichita State University, USA, (2007).
- [8] ANSYS AUTODYN User's Manual Theory manual, ANSYS Inc. Southpointe, 275 Technology Drive, Canonsburg, PA, USA, (2010).
- [9] BENSON, D.J.: *An efficient, accurate, simple ALE method for nonlinear finite element programs*, Computer Methods in Applied Mechanics and Engineering, 1989, 72, pp.305-350.
- [10] HEIMBS, S.: *Bird strike simulations on composite aircraft structures*, 2011 SIMULIA Customer Conference, Barcelona, Spain, May 17-19, 2011, pp.73-86.
- [11] GUIDA, M., MARULO, F., MEO, M., RICCIO, M., RUSSO, S.: *Fiber metal laminate for bird impact conditions*, Numerical and experimental analysis, Proceedings of ICCST/6, Durban, South Africa, (2007), pp CD-ROM.
- [12] BUDGEY, R.: *The development of a substitute artificial bird by the international bird strike research group for use in aircraft component testing*, Technical Report IBSC25/WP-IE3, International Bird Strike Committee, Amsterdam, (2000).
- [13] BLAIR, A.: *Aeroengine fan blade design accounting for bird strike*, PhD Dissertation, Department of Mechanical and Industrial Engineering, The University of Toronto, Canada, (2008).

Received: 07.09.2012.

## Primena hidrodinamičke teorije i metode konačnih elemenata u analizi udara ptice u ravnu prepreku

U oba slučaja dve metode odnosno teorije, hidrodinamičke teorije i metode konačnih elemenata, telo ptice je modelovano kao porozni materijal sastavljen od vode i vazduha u obliku cilindra sa ravnim ili polusfernim krajevima. Modelovanje ptice konačnim elementima je izvršeno primenom SPH (Smooth Particle Hydrodynamics) metode za materijal različite poroznosti. U tom cilju, definisana je zavisnost brzine zvuka i zapreminskog modula elastičnosti od poroznosti u jednačini stanja materijala. Takođe, predložen je i novi pristup proračunu zaustavnog pritiska u poroznom materijalu. Na drugoj strani, Lagranžova meta je razmatrana kao jednostavna ravna čelična kruta ili elastična ploča od legure aluminijuma. Data je komparativna analiza proračunskih rezultata udara ptice dobijenih primenom Igonijeve teorije udara i SPH metode. Takođe, izneti su i određeni eksperimentalni podaci.

*Ključne reči:* udar, mehanički udar, ptice, modelovanje, simulacija procesa, metoda konačnih elemenata, hidrodinamička teorija.

## Применение гидродинамической теории и метода конечных элементов для анализа удара птиц в плоский барьер

В обоих случаях применения двух методов или двух теорий, гидродинамической теории и метода конечных элементов, тело птицы моделируется как пористый материал, состоящий из воды и воздуха в виде цилиндра с плоскими или с полусферичными концами. Моделирование птиц методом конечных элементов было сделано при помощи SPH (Smooth Particle Hydrodynamics) метода для материалов различных пористости. С этой целью и определена зависимость скорости звука и модуля объёмной упругости от пористости материала в уравнении состояния материала. Также предложен и новый подход для расчёта тормозного давления в пористом материале. С другой стороны, мишень-цель Лагранжа рассматривается как простая полосовая стальная жёсткая пластина или упругая пластина из алюминиевого сплава. Здесь приведён сравнительный анализ расчётных результатов удара птиц, полученных применением теории удара Игония и SPH метода. Также представлены и определённые экспериментальные данные.

*Ключевые слова:* удар, механический удар, птицы, моделирование, моделирование процессов, анализ методом конечных элементов, гидродинамическая теория.

## **Application de la théorie hydrodynamique et de la méthode des éléments finis dans l'analyse de l'impact d'oiseau contre un obstacle plat**

Dans les deux cas d'application des deux méthodes ou théories, les théories thermodynamique et celle des éléments finis, le corps d'oiseau a été modélisé en matériel poreux composé de l'eau et de l'air en forme cylindrique aux bouts plats ou hémisphériques. La modélisation de l'oiseau à l'aide des éléments finis a été réalisée par la méthode SPH (Smooth Particle Hydrodynamics) pour le matériel de différente porosité. On a défini à cet effet la dépendance de la vitesse de son et du module volumétrique d'élasticité de la porosité dans l'équation de l'état de matériel. On a proposé aussi une nouvelle approche à la computation de la pression de stagnation chez le matériel poreux. De l'autre côté, la cible de Lagrange a été considéré comme une simple plaque plate en acier, rigide ou élastique, en alliage d'aluminium. On a présenté une analyse comparée des résultats numériques de l'impact d'oiseau obtenus par l'application de la théorie de Hugoniot et de la méthode SPH. On a présenté aussi certaines données expérimentales.

*Mots clés:* impact, impact mécanique, oiseaux, modélisation, simulation du processus, méthode des éléments finis, théorie hydrodynamique.